Superconductivity of monolayer Mo$_2$C: the key role of functional groups

Jun-Jie Zhang[1] and Shuai Dong[1, a)]

Department of Physics, Southeast University, Nanjing 211189, China

(Dated: 4 October 2018)

Monolayer Mo$_2$C is a new member of two-dimensional materials. Here the electronic structure and lattice dynamics of monolayer Mo$_2$C are calculated. According to the electron-phonon interaction, it is predicted that monolayer Mo$_2$C could be a quasi-two-dimensional superconductor and the effects of functional-groups are crucially important considering its unsaturated surface. Despite the suppressed superconductivity by chalcogen adsorption, our most interesting prediction is that the electron-phonon interaction of monolayer Mo$_2$C can be greatly enhanced by bromine absorbtion, suggesting that Mo$_2$CBr$_2$ as a good candidate for nanoscale superconductor.

I. INTRODUCTION

Two-dimensional (2D) graphene-like carbides and carbonitrides (MXenes, e.g. Ti$_2$C and Nb$_2$C) have attracted enormous interest for their novel chemical and physical properties, since they were successfully produced by etching the A layers of MAX phase (M is an early transition metal, A is an element from group IIIA or IVA, and X is carbon or nitrogen)[1–3]. Due to the unsaturated surface with unpaired electrons, the surfaces of MXenes always easily adsorb various functional groups (e.g. F, O, or/and OH group) during etching, thus the chemical and physical properties are varying with various adsorptions. For this reason, MXenes and their functionalized ones have been widely investigated regarding the magnetism, electronic structures, as well as catalytic properties and energy storage[4–8].

Recently, 2D layered Mo$_2$C as a new member of MXenes was formed from Mo$_2$Ga$_2$C thin films. The metallic nature of Mo-Ga bond is weaker than Mo-C bond which has a mixed covalent/metallic/ionic character, thus monolayer Mo$_2$C can be produced by selectively etching Ga layer[9]. Structurally, monolayer Mo$_2$C is constructed by the Mo-C-Mo sandwich, as shown in Fig. 1(a), which looks similar to 1T-MoS$_2$. Khazaei *et. al.* studied the thermoelectrics properties of monolayer Mo$_2$C, which was found to be a promising candidate as a high-performance thermoelectric material[10]. In addition, the structural, electrical, thermal and mechanical properties of monolayer Mo$_2$C were also studied[11].

Superconductivity in ultrathin films owns promising future for applications, e.g. superconducting computational devices, thus great efforts have been made to discover 2D superconductors[12–14]. Considering that monolayer Mo$_2$C is non-magnetic and appears strong metallicity (according to first-principles study)[10], it brings the opportunity to be an ultrathin superconductor. However, although the superconductivity was discovered in bulk α-Mo$_2$C (an allotrope of 2D layered Mo$_2$C), its superconducting transition temperature (T_C) was depressed from
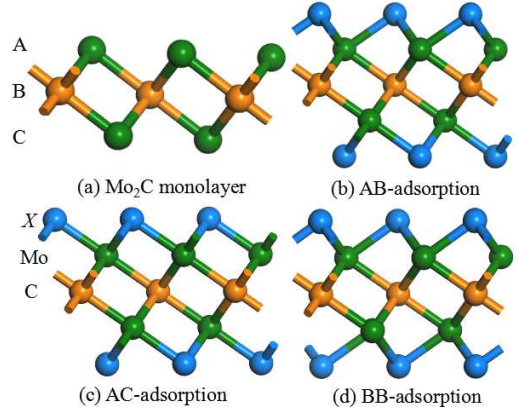
FIG. 1. Side views of atomic structures of monolayer Mo$_2$C (a) and three atom-adsorbed configurations (b)-(d).

4 K (thick film) to near 0 K when its thickness is less than 3.5 nm[15,16]. Moreover, analogous to other members of MXenes, the surfaces of monolayer Mo$_2$C are easily covered by functional groups, and Khazaei *et. al.* indicates the full adsorption of functional groups is more stable than the cases of partial adsorption[17]. For multilayer Mo$_2$C MXenes, they (stacking like MoS$_2$) seem to be impossible due to its unsaturated surfaces. In experiments, the possible stackings are -Mo$_2$CX$_2$-Mo$_2$CX$_2$- and Mo-C-Mo-C-Mo. For the former, the effects of functional groups are unavoidable. For the latter, the stoichiometry has changed. These facts motive us to investigate the superconductivity of pure Mo$_2$C monolayer and those with various functional groups.

In this work, the lattice dynamics and electron-phonon coupling (EPC) of monolayer Mo$_2$C and functionalized ones have been studied via first-principles density functional theory (DFT) and density function perturbation theory (DFPT). Our calculations find that the strong EPC in monolayer Mo$_2$C may lead to superconductivity, while the oxidation would make its superconductivity disappear. Besides, the superconducting T_C is also obviously suppressed by absorbtion of sulfur or selenium. In contrast, the EPC of monolayer Mo$_2$C can be greatly enhanced by bromine absorbtion, leading to a predicted T_C up to 12 K.

a)Electronic mail: sdong@seu.edu.cn

II. MODEL & METHODS

The electronic structure calculations have been performed using the Vienna *ab initio* simulation package (VASP) with projector augmented wave method[18,19]. Generalized gradient approximation of Perdew-Burke-Ernzerhof (GGA-PBE) are used with a cutoff energy 600 eV. The spin-orbit coupling (SOC) is also included in electronic structure calculations. The phonon dispersion calculations are carried out using ultrasoft pseudopotential (including the semicore electrons as valence electrons in case of Mo) as implemented in PWSCF program of the Quantum-ESPRESSO distribution, which are calculated within the framework of DFPT[20]. In the DFPT calculation, GGA-PBE formulation is also used with a cutoff energy 35 Ry for the expansion of the electronic wave function in the plane waves, whereas cutoff energy for charge density and potential is set to be 350 Ry. Structure optimization and electronic structure are repeated by using PWSCF and the results are consistent with those obtained using VASP.

The vacuum space of ~ 15 Å is intercalated into interlamination to eliminate the interaction between layers. A 12×12 2D grid uniform is applied for both the k-points of the self-consistent and q-points of dynamical matrices calculations.

The EPC calculation is estimated according to the Migdal-Eliashberg theory [$\alpha^2 F(\omega)$], which is given by[21]:

$$\alpha^2 F(\omega) = \frac{1}{2\pi N(\varepsilon_F)} \sum_{\mathbf{q}\nu} \delta(\omega - \omega_{\mathbf{q}\nu}) \frac{\gamma_{\mathbf{q}\nu}}{\hbar \omega_{\mathbf{q}\nu}} \quad (1)$$

where $N(\varepsilon_F)$ is the electronic DOS at Fermi level, $\omega_{\mathbf{q}\nu}$ denotes phonon frequency of the νth phonon mode with wave vector $\mathbf{q}$, and the phonon linewidth $\gamma_{\mathbf{q}\nu}$ is defined by[22,23]:

$$\gamma_{\mathbf{q}\nu} = \frac{2\pi \omega_{\mathbf{q}\nu}}{\Omega_{BZ}} \sum_{ij} \int d^3k \left| g_{\mathbf{ki},\mathbf{k}+\mathbf{qj}}^{\mathbf{q}\nu} \right|^2 \delta(\varepsilon_{\mathbf{ki}} - \varepsilon_F)$$
$$\times \delta(\varepsilon_{\mathbf{k}+\mathbf{qj}} - \varepsilon_F). \quad (2)$$

where ij denote indices of energy bands, Ω_{BZ} is volume of Brillouin zone, $\varepsilon_{\mathbf{ki}}$ and $\varepsilon_{\mathbf{k}+\mathbf{qj}}$ are eigenvalues of Kohn-Sham orbitals at given bands and wave vectors. The $g_{\mathbf{k},\mathbf{q}\nu}$ is the EPC matrix element which can be determined self-consistently by the linear response theory, which describes the probability amplitude for scattering of an electron with a transfer of crystal momentum $\mathbf{q}$, is determined by[22,23]:

$$g_{\mathbf{k},\mathbf{q}\nu}^{ij} = \left(\frac{\hbar}{2M\omega_{\mathbf{q}\nu}}\right)^{1/2} \langle \psi_{i,\mathbf{k}} | \frac{dV_{SCF}}{d\hat{u}_{\mathbf{q}\nu}} \cdot \hat{e}_{\mathbf{q}\nu} | \psi_{i,\mathbf{k}+\mathbf{q}} \rangle \quad (3)$$

where M is the atomic mass, $\frac{dV_{SCF}}{d\hat{u}_{\mathbf{q}\nu}}$ measures the change of self-consistent potential induced by atomic displacement, $\psi_{i,\mathbf{k}}$ and $\psi_{i,\mathbf{k}+\mathbf{q}}$ are Kohn-Sham orbitals.

The EPC constant λ is obtained by summation over the first Brillouin zone or integration of the $\alpha^2 F(\omega)$ in the $\mathbf{q}$ space[22,23]:

$$\lambda = \sum_{\mathbf{q}\nu} \lambda_{\mathbf{q}\nu} = 2 \int_0^\infty \frac{\alpha^2 F(\omega)}{\omega} d\omega \quad (4)$$

where EPC constant $\lambda_{\mathbf{q}\nu}$ for mode ν at wave vector $\mathbf{q}$ is defined by the integration[22,23]:

$$\lambda_{\mathbf{q}\nu} = \frac{\gamma_{\mathbf{q}\nu}}{\pi \hbar N(\varepsilon_F) \omega_{\mathbf{q}\nu}^2}. \quad (5)$$

To obtain accurate electron-phonon interaction matrices, a dense $36 \times 36 \times 1$ grid is adopted for the EPC calculation.

III. RESULTS & DISCUSSION

A. Unfunctionalized monolayer Mo₂C

The structure of unfunctionalized monolayer Mo_2C is layered hexagonal with a space group of D_{3d}, and the stacking of the Mo-C-Mo is in the ABC-type along the hexagonal c axis (see Fig. 1(a)), which is similar to 1T-MoS_2. Our optimized lattice constant (2.965 Å) is consistent with the value reported by Khazaei *et. al.*[10].

The calculated band structures and density of states (DOS) are shown in Fig. 2. As previously reported[10], monolayer Mo_2C indicates strong metallic behavior, and the Fermi surfaces are mainly contributed by Mo's d-orbits according to the projected DOS (Fig. 2(a)). The maximally localized Wannier functions (MLWFs) can partion Mo's d orbital and C's p orbital, as shown in Fig. 2(b). C's p orbital is mainly occupied on energy range from -8 eV to -4 eV and highly hybridize with Mo's d orbitals. The p_x and p_y orbitals are degenerate, which are higher in energy than the p_z orbital, as shown in Fig. 2(a). The Mo's d-orbital are split due to C_{3v} crystalline field. Thus the d_{z^2} has the lowest on-site energy, the rests are pairwise degenerate: ($d_{x^2-y^2}$ and d_{xy}) and (d_{xz} and d_{yz}), the later of which is sightly higher. The SOC can open the degeneracy at $\bar{\Gamma}$ point (see Fig. 2(c)), while it has little effect on the Fermi surface. The crossing-Fermi-level bands and corresponding Fermi surfaces are shown in Fig. 2(d) and (e). The anti-bonding d_{z^2} band (the upper one in Fig. 2(e)) forms the hole pocket Fermi surfaces around $\bar{M}$ points, while the electron Fermi surface (the lower one in Fig. 2(e)) is the circular-shape around the $\bar{\Gamma}$ point which is mainly contributed by $d_{x^2-y^2}$ and d_{xy}. Such double Fermi surfaces correspond to carriers with multiple effective masses, charges, and mobilities.

Then the phonon properties and electron-phonon coupling are calculated. The SOC is not included in these calculations, considering its negligible effects on the Fermi surfaces. For monolayer Mo_2C, the Raman modes can be decomposed as $A_{1g}^1 \oplus 2E_g^1$ at the zone center (see Fig. 3(a)), and the calculated Raman frequencies are 150.3 cm^{-1} and 193.1 cm^{-1} for the E_g^1 and A_{1g}^1 modes respectively. Moreover, both Raman modes have strong
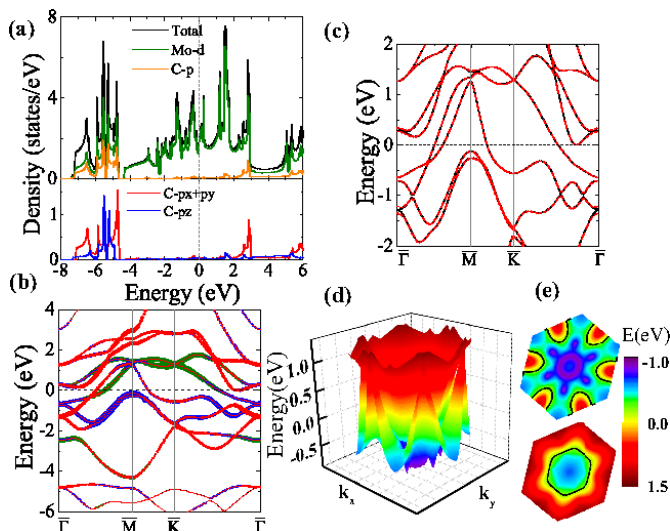
FIG. 2. Electronic structure of monolayer Mo_2C. (a) Density of states (DOS) and Projected DOS. (b) Projected band structure. Red: d_{z^2}; Green: $d_{x^2-y^2}$ and d_{xy}, Blue: d_{xz} and d_{yz}. (c) Band structure with (black) and without SOC (red). (d) Three-dimensional view of two bands cross the Fermi level. (e) Energy couterplots of two bands. Black curves: the Fermi surface.

FIG. 3. Phonon properties for single Mo_2C layer. (a) Calculated phonon dispersion. Insert: sketch of Raman modes. (b-c) Phonon DOS, electron-phonon coupling λ, and Eliashberg spectral function.

coupling to electrons ($\lambda_{\mathbf{q}\nu}$ is 0.11 for E_g^1 and 0.21 for A_{1g}^1) according to Eq. 5.

The calculated phonon dispersions along major high symmetry lines and phonon densities of states (PDOS, $F(\omega)$) for monolayer Mo_2C are shown in Fig. 3(a). More dense k-meshes ($18 \times 18 \times 1$ and $24 \times 24 \times 1$) in self-consistent calculations are also tested. The maximum error of obtained phonon frequencies are less than 1%, implying the convergence of phonon calculation. In addition, the different methodology and pseudo-potential would lead to a few differences regarding the phonon band structures[8,11]. In fact, our phonon structure is very close to that in previous report[11], although tiny differences remain unavoidable.

No imaginary frequency exists in the full phonon spectra, indicating the dynamical stability of monolayer Mo_2C. Meanwhile, the phonon behavior exhibits several remarkable characteristics. First, near the zone center, both the LA and TA branches are near linear while the ZA branch (out-of-plane acoustical mode) is quadratic. These characters reflect the nature of 2D sheet. In detail, the ZA phonon in 2D materials like graphene has a quadratic dispersion over a wide range of the 2D Brillouin zone $\omega_{ZA} = a_{ZA}q^2$, where a_{ZA} is a positive constant and q is the 2D phonon wave vector. The similar conclusions are also found in monolayer black phosphorene[24]. Second, according to the partial PDOS (Fig. 3(b)), the vibrational modes of Mo dominate the low-frequency regime while those of C dominate the high-frequency regime, due to their large difference in mass. There is a large gap around 300 cm^{-1}, which partions the optical modes of Mo and C.

To discuss the superconductivity, the obtained $\alpha^2F(\omega)$ and $\lambda(\omega)$ are also plotted in Fig. 3(c). Their similar shapes indicate that all $F(\omega)$ make contributions to EPC. Due to the factor $1/\omega$ in the definition of λ (see Eq. 4), the contributions from low ω region is more prominent. Exactly, the calculated $\lambda(\omega = 250 \text{ cm}^{-1})$ is ≈ 0.56 which is beyond 90% of the total EPC ($\lambda(\omega = \infty) = 0.63$), indicating that the phonon modes in the frequency region below 250 cm^{-1} have the dominant contribution. In particular, three low-lying optical branches have strong coupling to electrons, which make 40% contribution to EPC. Therefore, it is natural to expect the strong EPC in monolayer Mo_2C to induce superconducting state. The T_C can be estimated using the Allen-Dynes modified McMillan equation[22]:

$$T_C = \frac{\omega_{ln}}{1.2} \exp[-\frac{1.04(1+\lambda)}{\lambda - \mu^*(1+0.62\lambda)}],$$ (6)

where μ^* is the Coulomb repulsion parameter and ω_{ln} is the logarithmically averaged frequency. When taking a typical value $\mu^* = 0.1$, the estimated T_C is about 5.9 K.

B. Functionalized monolayer Mo_2C

In above study, it has been predict that pure monolayer Mo_2C maybe a quasi-2D superconductor. However, in real situations, the functional group at surfaces of monolayer Mo_2C are unavoidable considering its highly unsaturated surfaces. In fact, previous studies reported that monolayer Mo_2C transforms from metal to semiconductor with F- and Cl-adsorption[10], namely the F- and Cl-functionalized monolayer Mo_2C could not be a superconductor. In the following, the changes of superconductivity by adsorbing various functional group will be studied, which may shed light to tuning the superconductivity of monolayer Mo_2C in real experiments.

Due to the full adsorption is more stable than the partial case[10], the 1×1 Mo_2C unit cell (u.c.) with two functional groups X (one on each surface), i.e. Mo_2CX_2, is adopted in our calculation. Four functional

TABLE I. The calculated total energy for Mo_2CX_2 of different configurations for adsorption is in unit of eV/per u.c.. The energy of BB-adsorption is set as the reference. The optimized lattice constant a is in unit of Å. For the most favorable configuration, the corresponding binding energy (E_b) (in unit of eV) is also presented.

	AB	AC	BB	a	a (Ref. 10)	E_b
O	0.72	1.29	0	2.891	2.886	−8.67
S	0.48	0.69	0	3.087	3.078	−6.08
Se	0.39	0.24	0	3.161		−4.57
Br	−0.19	−0.65	0	3.428	3.418	−3.13

TABLE II. The calculated Mo_2CX_2's superconductive parameters of $N(\varepsilon_F)$ (states/eV), ω_{ln} (K), λ, and T_C (K).

	Mo_2CO_2	Mo_2CS_2	Mo_2CSe_2	Mo_2CBr_2
$N(\varepsilon_F)$	1.3	1.5	1.6	3.3
ω_{ln}	357.4	326.6	283.7	160.7
λ	0.2	0.4	0.4	1.1
T_C	< 0.1	1.0	1.4	12.8

atoms (X=O, S, Se, and Br) are considered. Considering the symmetry, there are three mostly possible site-configuration for adsorption: AB-adsorption (Fig. 1(b)), AC-adsorption (Fig. 1(c)), BB-adsorption (Fig. 1(d)). For the AB-adsorption, one X atom is right above C layer, while another X is right below other side Mo. For the AC-adsorption, each X atom is right above/below other side Mo layer. For the BB-configuration, both two X atoms stand above/below the C site.

The crystal structures are fully relaxed upon the absorptions, and the calculated lattice constant as well as total energy are listed in Table I. Our calculations are in good agreement with previous reports[10,25], and the BB-adsorption is the most favorable case for chalcogen, while Mo_2CBr_2 favors the AC-adsorption. The corresponding binding energy ($E_b = E_{Mo_2CX_2} - E_{Mo_2C} - E_{X_2}$) is also calculated and also listed in Table I. All binding energies are negative which indicate thermodynamic stability for all structures. And the value of binding energy decreases from Mo_2CO_2 to Mo_2CBr_2, implying the adsorption of oxygen should be quite possible, as observed in real experiment[9]. According to the Löowdin population analysis, the charge transfer from Mo to X is about 0.48, 0.39, 0.34, and 0.24 electron for O-, S-, Se-, and Br-adsorption, respectively. Stronger Coulomb attraction between X and Mo ions can lead to larger binding energy.

The electronic structures for Mo_2CX_2 are calculated. Due to the unchanged symmetry of crystalline field, the splitting of Mo's d orbitals is similar to pristine monolayer Mo_2C. Quantitatively, the absorption of X further raises the energy of doubly-degenerate d_{xz} and d_{yz} due to the strong hybridization with the p orbitals of X. In details, the on-site energy difference between d_{xz}/d_{yz} and $d_{x^2-y^2}/d_{xy}$ is about 1.72, 0.99, 0.71, 0.21 eV for the O-, S-, Se- and Br-adsorption respectively, according to the MLWFs calculation. The lower of d_{xz}/d_{yz} orbitals can be also evidenced in the band structures of Mo_2CX_2, as shown in Fig. 4(a-d). All band structures show metallic character after X-absorption, different to previously studied F-/Cl-absorption. Similar to pristine monolayer Mo_2C, $d_{x^2-y^2}/d_{xy}$ and d_{z^2} of Mo still make dominant contributions around the Fermi level, although the contributions from $d_{x^2-y^2}/d_{xy}$ are reduced more or less, as

shown in Fig. 4(a-d). The three-dimensional view of three bands as well as the Fermi surface of $d_{x^2-y^2}/d_{xy}$ and d_{z^2} are shown in Fig. 4(e-h). For chalcogen, its band structure looks like that of pristine monolayer Mo_2C, namely the upper cone-shape band is surrounded by lower flower-shape band, although the degree of surrounding is suppressed. Due to the different adsorption site and valence state of Br, the shapes of Fermi surfaces are significantly changed to sun-like patterns for Mo_2CBr_2.

The calculated phonon dispersion along major high symmetry lines are shown in Fig. 5. No imaginary frequency exists in the full phonon spectra, indicating the dynamical stability of the Mo_2CX_2. Therefore, it is more likely that Mo_2CX_2 is able to be obtained in real experiment considering its stability in thermodynamics and lattice dynamical. Obviously, the vibration modes of Mo_2C are strongly coupled with the surface X, as revealed by the phonon dispersion (Fig. 5). Different X atom contribute to the phonon spectrum in different frequency range due to the inequivalent mass and bond strength. In particular, for Mo_2CO_2, the contributions from O mainly locate at the intermediate- and high-frequency regimes, indicating the fact of strong bond of Mo-O. In the case of Mo_2CS_2, the frequencies contributed by S mainly locate in the intermediate regime, while for Se and Br cases the contributions from X is in the low frequency side.

Our results for $\alpha^2F(\omega)$, $F(\omega)$ and PDOS of Mo_2CX_2 are shown in Fig. 6. As in the monolayer Mo_2C case, $\alpha^2F(\omega)$ and $F(\omega)$ of Mo_2CX_2 have similar peaks, indicating all vibration modes contribute to EPC. Comparing to pristine Mo_2C, the strength of $\alpha^2F(\omega)$ have been suppressed by O-, S- and Se-adsorption. And such suppression obviously exists in low frequency regime which have large contributions to EPC (because of the ω^{-1} part in Eq. 4). The average EPC is also calculated using Eq. 4, as listed in Table II. Corresponding T_C is estimated from modified McMillan equation (Eq. 6) with $\mu^* = 0.1$ (listed in Table II). The results indicate that the superconductivity is greatly suppressed in Mo_2CS_2 and Mo_2CSe_2 and almost disappears in Mo_2CO_2, as a result of reduced electronic DOS's at Fermi level and suppressed EPC's.

As shown in Fig. 6(d), strength of $\alpha^2F(\omega)$ has been improved in Mo_2CBr_2, and the corresponding average EPC is about 1.09. The obtained $\lambda(\omega = 300$ cm$^{-1}) \approx 0.97$ is approximately beyond 88% of the total EPC ($\lambda(\omega = \infty) = 1.09$), and estimated T_C is up to 12.8 K. To be exact, EPC of vibration modes (E_g^1 and A_{1g}^1) at $\bar{\Gamma}$ point
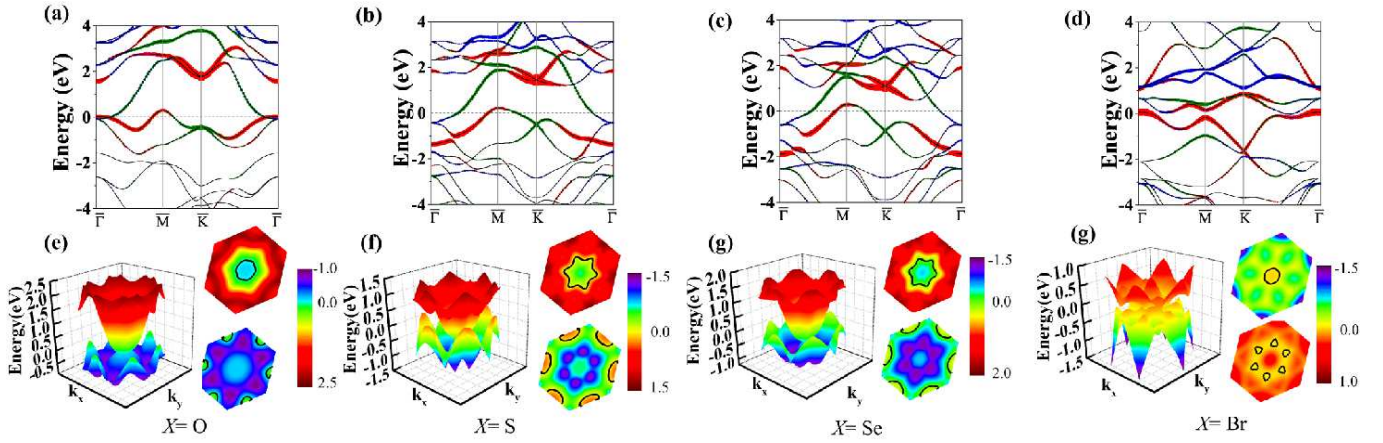
FIG. 4. Electronic structures of Mo_2CX_2. (a-d) Band structures. Red: d_{z^2}; Green: $d_{x^2-y^2}$ and d_{xy}; Blue: d_{xz} and d_{yz}. (e-h) Three-dimensional view of three bands around the Fermi level and the corresponding Fermi surface (Black curves).
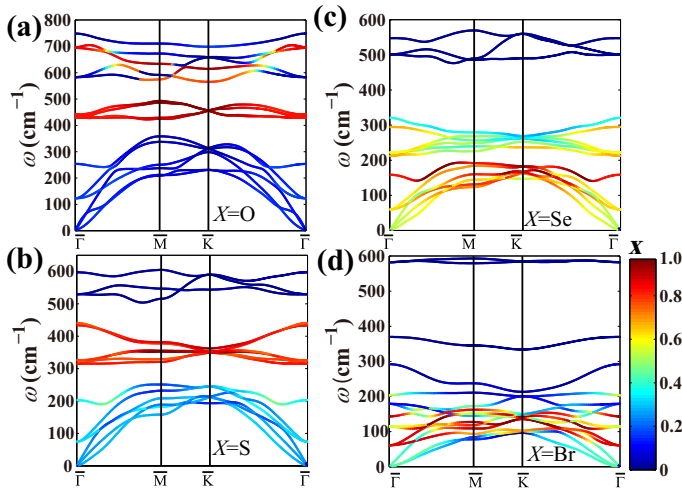
FIG. 5. Calculated phonon dispersion for Mo_2CX_2. The contribution from X and monolayer Mo_2C is distinguished by color.
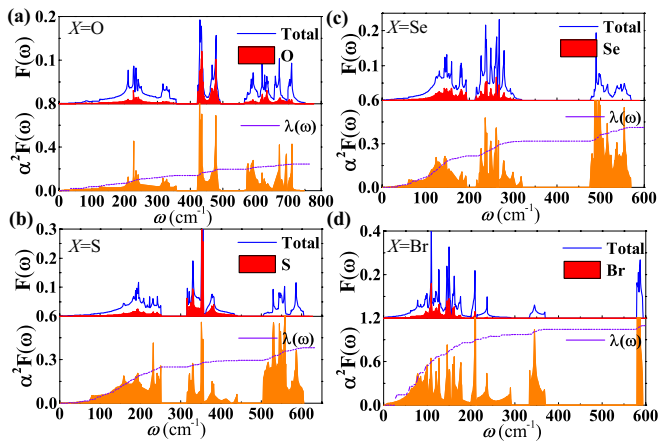
FIG. 6. Phonon DOS (PDOS, $F(\omega)$), projected PDOS of X atoms, electron-phonon coupling $\lambda(\omega)$, and Eliashberg spectral function of Mo_2CX_2.

which have Raman activity have been improved for 30% comparing to those of pristine monolayer Mo_2C. In addition, the large values of EPC for acoustic modes at $\bar{M}$ contribute substantially to the average EPC. Thus, the superconductive T_C is pushed up in Mo_2CBr_2.

In addition, we had tried the full -OH cover up Mo_2C surfaces. However, even after the atomic relaxation, an imaginary frequency of phonon appears at the $\bar{M}$ point, implying unstable structure. Therefore, structural phase transition would appear which makes the problem more complicated. Thus, the decoration of OH group is beyond the current work and deserves individual studies in future.

IV. CONCLUSION

We have analyzed the electronic properties, the lattice dynamical properties, and superconductivity of monolayer Mo_2C and its functionalized ones. Our calculations have confirmed the strong EPC in monolayer Mo_2C, which may lead to superconductivity below 5.9 K. Even though, since the absorption of functional groups is unavoidable in real experiment, its superconductivity can be modified. Our calculation have found that for chalcogen functionalized monolayer Mo_2C the superconductivity would be seriously suppressed (or even totally disappear). The most interesting prediction is that electron-phonon coupling can be greatly enhanced in monolayer Mo_2C by bromine absorbtion, and thus its corresponding superconductive T_C may be pushed up to 12.8 K, suggesting that Mo_2CBr_2 may be a good candidate as nanoscale superconductor.

[1] M. Naguib, M. Kurtoglu, V. Presser, J. Lu, J. Niu, M. Heon, L. Hultman, Y. Gogotsi, and M. W. Barsoum, Adv. Mater. **23**, 4248 (2011).

[2] M. Naguib, O. Mashtalir, J. Carle, V. Presser, J. Lu, L. Hultman, Y. Gogotsi, and M. W. Barsoum, ACS nano **6**, 1322 (2012).

[3] M. Naguib, J. Halim, J. Lu, K. M. Cook, L. Hultman, Y. Gogotsi, and M. W. Barsoum, J. Am. Chem. Soc. **135**, 15966 (2013).

[4] M. R. Lukatskaya, O. Mashtalir, C. E. Ren, Y. Dall'Agnese, P. Rozier, P. L. Taberna, M. Naguib, P. Simon, M. W. Barsoum, and Y. Gogotsi, Science **341**, 1502 (2013).

[5] S. Zhao, W. Kang, and J. Xue, Appl. Phys. Lett. **104**, 133106 (2014).

[6] M. Khazaei, M. Arai, T. Sasaki, C.-Y. Chung, N. S. Venkataramanan, M. Estili, Y. Sakka, and Y. Kawazoe, Adv. Funct. Mater. **23**, 2185 (2013).

[7] M. Ghidiu, M. R. Lukatskaya, M.-Q. Zhao, Y. Gogotsi, and M. W. Barsoum, Nature **516**, 78 (2014).

[8] W. Sun, Y. Li, B. Wang, X. Jiang, M. I. Katsnelson, P. Korzhavyi, O. Eriksson, and I. Di Marco, Nanoscale **8**, 15753 (2016).

[9] R. Meshkian, L.-Å. Näslund, J. Halim, J. Lu, M. W. Barsoum, and J. Rosen, Scripta Mater. **108**, 147 (2015).

[10] M. Khazaei, M. Arai, T. Sasaki, M. Estili, and Y. Sakka, Phys. Chem. Chem. Phys. **16**, 7841 (2014).

[11] X.-H. Zha, J. Yin, Y. Zhou, Q. Huang, K. Luo, J. Lang, J. S. Francisco, J. He, and S. Du, J. Phys. Chem. C **120**, 15082 (2016).

[12] J.-F. Ge, Z.-L. Liu, C. Liu, C.-L. Gao, D. Qian, Q.-K. Xue, Y. Liu, and J.-F. Jia, Nature Mater. **14**, 285 (2015).

[13] J.-J. Zhang, B. Gao, and S. Dong, Phys. Rev. B **93**, 155430 (2016).

[14] J.-J. Zhang and S. Dong, 2D Mater. **3**, 035006 (2016).

[15] C. Xu, L. Wang, Z. Liu, L. Chen, J. Guo, N. Kang, X.-L. Ma, H.-M. Cheng, and W. Ren, Nature Mater. **14**, 1135 (2015).

[16] M. K. Kolel-Veetil, S. B. Qadri, M. Osofsky, T. M. Keller, R. Goswami, and S. A. Wolf, J. Phys. Chem. C **111**, 16878 (2007).

[17] Y. Xie and P. R. C. Kent, Phys. Rev. B **87**, 235441 (2013).

[18] G. Kresse and J. Furthmüller, Phys. Rev. B **54**, 11169 (1996).

[19] G. Kresse and D. Joubert, Phys. Rev. B **59**, 1758 (1999).

[20] P. Giannozzi, S. Baroni, N. Bonini, M. Calandra, R. Car, C. Cavazzoni, D. Ceresoli, G. L. Chiarotti, M. Cococcioni, and I. D. et al., J. Phys.: Condens. Matter **21**, 395502 (2009).

[21] G. Grimvall, *The electron-phonon interaction in metals*, Vol. 8 (North-Holland Amsterdam, 1981).

[22] P. B. Allen and R. C. Dynes, Phys. Rev. B **12**, 905 (1975).

[23] P. Allen, Phys. Rev. B **6**, 2577 (1972).

[24] G. Qin, Q.-B. Yan, Z. Qin, S.-Y. Yue, M. Hu, and G. Su, Phys. Chem. Chem. Phys. **17**, 4854 (2015).

[25] H. Weng, A. Ranjbar, Y. Liang, Z. Song, M. Khazaei, S. Yunoki, M. Arai, Y. Kawazoe, Z. Fang, and X. Dai, Phys. Rev. B **92**, 075436 (2015).